A Comprehensive Overview of Spectrometers:
Calculating the index of refraction of air and finding the spacing between Sodium-D emission lines

January 29, 2020
Report by Xavier Boluna
Laboratory partner: Ryota Johnson

ABSTRACT

This report covers four basic interferometers and discusses their different features, specialized applications and helpful methods to build and calibrate them. These are the Michelson, Sagnac, Mach-Zederman and Fabry-Perot interferometers.

As part of an investigation into their unique properties, we measured the refractive index of air using different configurations of the Michelson and the Mach-Zederman interferometers. For the Michelson Interferomter, we collected two sets of data -- one with equal-length arms and the other without -- to calculate refractive indexes of air $(1 + 269.09 \times 10^{-6}) \pm (1.28 \times 10^{-6})$and $(1 + 267.07 \times 10^{-6}) \pm (1.11 \times 10^{-6})$, respectively. The Mach-Zederman's calculated value came to $(1 + 265.45 \times 10^{-6}) \pm (0.68 \times 10^{-6})$. The p-values for all three of these calculated values were practically zero, indicating a significant disagreement. Upon closer analysis suggests systematic error, however, and more experimentation is suggested to resolve these problems.

We used the Fabry-Perot interferometer to measure the spacing of emission wavelengths of a Sodium-D lamp. We calculated a value of 0.5978 ± 0.0058 nm and a p-value of 0.4698, indicating signficant agreement.

Interference patterns from the Michelson (top right), Fabry-Perot (bottom right) and Sagnac (below) Interferometers.

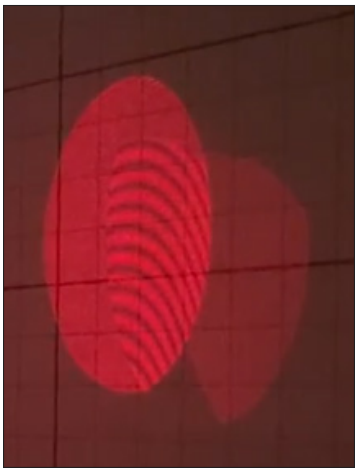

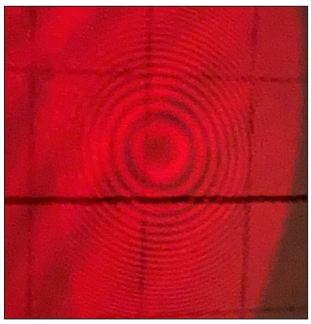

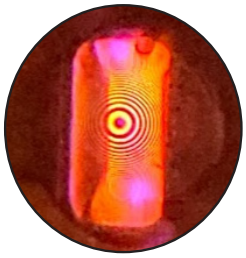

Exploration of the Mach-Zederman Interferometer's ability to show images of the change in the refractive index of air.

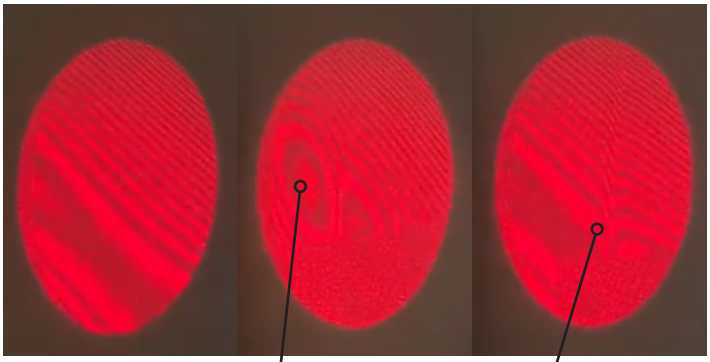

Without any changes, an interference pattern.

A lighter flame held in front of the beam.

A stream of butane held in front of the beam.

Introduction

Spectroscopy owes its genesis to one of the most contentious questions of the 19th century: how did electromagnetic waves travel through space? Many of the most prolific physicists of the time dealt with this question, including Maxwell, who built his family of equations on the existence of an 'ether' which permuted matter and through which light could propagate.

Such was the state of physics when Albert Michelson and Edward Morley created their now historied experiment: an interferometer oriented in parallel to the Earth, to measure the planet's drift through this stationary ether (see Figure Two, next page). As the Earth rotated on its axis, the fringes created by optical interference should shift slowly -- thereby allowing them to measure the Earth's absolute velocity through this substance (Feynman, 1963).

Michelson & Morley's experiment bore results which remained unexplained for nearly two decades, until Albert Einstein's development of relativity proved that their measurement was correct. The Earth's absolute velocity through the ether was zero, because the ether did not exist.

The science of spectroscopy is fundamental to the trajectory of modern physics. In the time since Michelson & Morley's experiment in 1887, spectrometers have reached ubiquity in the world of scientific instrumentation. Various different types exist, including those in hospitals (see MRI machines), forensics laboratories (see Mass Spectrometers) and aboard rovers bound for Mars (see Opportunity's tri-color imaging spectrometer). In October of 2017, the Laser-Interferometer Gravitational-Wave Observatory used two massive interferometers placed on the limits of the contiguous U.S. to measure the collision of two black holes more than a billion light-years away from Earth (LIGO, Caltech).

The interferometers that measured this event were, at their core, Michelson interferometers. This report explores this interferometer, among other modifications which constitute the Mach-Zedner, Sagnac and Fabry-Perot interferometers. These interferometers are each functionally equivalent to the specialized systems found in applications around the world.

We explore some of these capacities, including the ability to measure the refractive index of air and sodium-D spectral emission doublet lines, fundamental in the discovery of the Zeeman effect (Lab Manual, Brown).

The goal of this report is to explore these interferometers and their properties, compare them to the scientifically accepted data and provide useful information to reproduce each experiment.

This report is organized in the following sections, including data tables and bibliographical information placed in the Appendix:

An abstract depiction of the 'Luminous Ether'

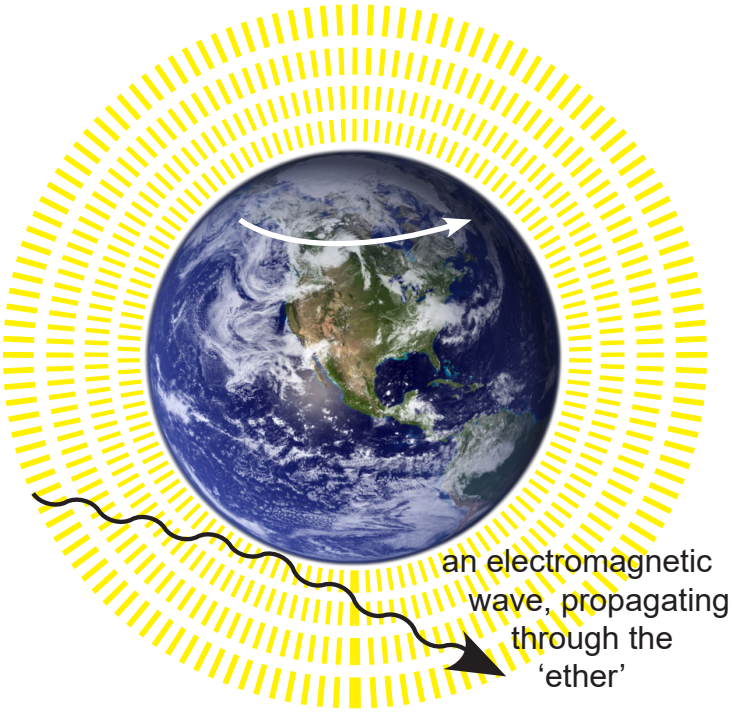

The Luminous Ether (fictionally pictured in yellow) was a hypothesized medium by which electromagnetic waves (including light) propagated. It was said to be in a stationary reference frame.

Michelson & Morley hypothesized that, by building an interferometer with an arm in parallel to the Earth's rotation (white arrow), they could measure the phase change as the Earth travelled through the ether. Their experiment yielded a transformative end result: the ether does not exist.

Methods and Procedures

Perhaps the most important and tedious process of building a spectrometer is its alignment. All four of our spectrometers require relatively precise alignment in order to create a resolved interference pattern.

The first step in aligning an interferometer is understanding the behavior of light interference. Any electromagnetic wave has the intrinsic property of wavelength and phase. In our case, we can consider coherent light, or light of a known and relatively fixed wavelength and phase. Like overlapping waves in the ocean, light interference creates regular fringes of constructive and destructive interference. Figure One is an excellent example, depicting the interference pattern produced by a Michelson Interferometer.

Figure Two depicts the schematic of a Michelson Interferometer. An important factor to regard is the wavelength of our emitted light. Our helium-neon laser is single-mode, meaning that just one wavelength of light is emitted at 632.8 nanometers, or 6,382 × 10^{-10} meters. This laser enters the beam expander (focal length (f) = 4.5mm), increasing its diameter, and reaches a half-silvered mirror known as the beam splitter. Oriented 45° to the laser, an ideal splitter evenly splits the light in two directions of equal intensity.

The distance between the beam splitter and the mirror is the arm length. This is crucial as, unless the arms are calibrated to a equal distance to a resolution of roughly 10^{-10} meters, the reflected lasers will not meet the beam splitter in phase. Slight differences in the path between the splitter and mirror, however, shift the fringes as the light intersects at different phases.

The methodology for finding the refractive index of air is to pressurize a tube of a certain length (ours is 20 cm), thereby increasing the refractive index, and counting the number of fringes that pass as the tube depressurizes. Theorem One (next page) derives the mathematical formula to describe the relationship between the number of fringes, the starting and ending air pressures and the refractive index of the gas.

We are able to perform this analysis of the refractive index with both the Michelson and Mach-Zedner interferometers, using the same equation for each.

Figure One: An interference pattern produced by our Michelson interferometer

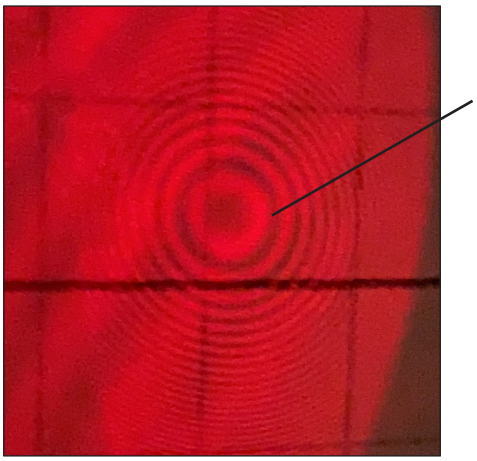

This is a picture of the interference pattern produced by the Michelson Interferometer. Notice the dark fringes, telltale of destructive interference. The fringes shift as the path length, and therefore the phase at the point of contact, change.

Figure Two: A simple schematic of the Michelson Interferometer

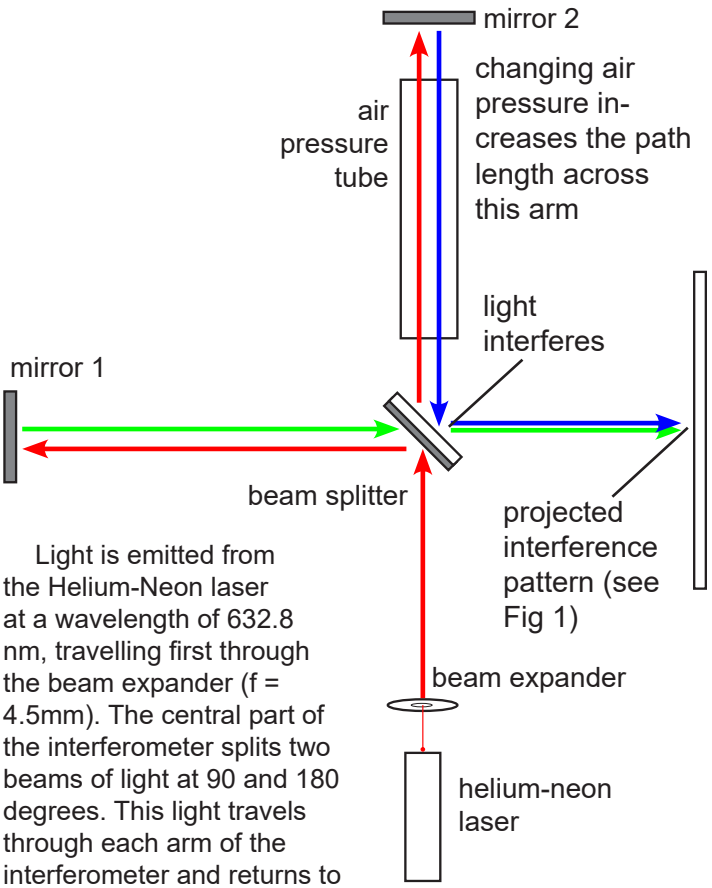

Light is emitted from the Helium-Neon laser at a wavelength of 632.8 nm, travelling first through the beam expander (f = 4.5mm). The central part of the interferometer splits two beams of light at 90 and 180 degrees. This light travels through each arm of the interferometer and returns to coincide on the beam splitter, which reflects the light towards a screen.

Each of the interferometers will now be discussed in turn, including the process of calibrating the interferometer and practical advice for accurately doing so.

The Michelson Interferometer

The crucial elements of the Michelson Interferometer have already been discussed above. Light emitted by the laser is expanded such that, incident on the beam splitter, a reflection and a transmission are directed upon each arm. That arm reflects the light which, incident again upon the beam splitter, interfere to create the pattern shown in Figure One.

Our particular experiment measures the refractive index of air and includes an air pressure tube on one of the arms, used to vary the light's path length and thereby that arm's phase upon reaching the beam splitter.

Pertinent to the experiment, both the factory rating and our own independent measurements evaluated the tube length at exactly 20 centimeters.

Figure Three shows our interferometer overlaid with its schematic. There are a few considerations when calibrating this interferometer.

First, ensure that all the elements are aligned such that the beam is parallel to the table at all times. This can be checked by measuring the laser height at every point along the interferometer.

Starting with a level laser beam makes all the difference when one begins to reflect the beams. With each mirror, attempt to place the mirror's reflection directly upon the original beam's origin on the beam splitter. If both dots overlap, the intensity should increase slightly. Doing so with both mirrors should readily produce an interference pattern on the screen.

From here, we can pressurize the tube and count the number of fringes that pass and utilize the equations from Theorem One to determine the refractive index of air.

Theorem One: Derivation of the relationship between Refractive Index, Pressure and the Number of Fringes

Consider γ to be the change in path length.

γ is equivalent to the number of fringes that pass multiplied by the wavelength (distance between phases) of the laser.

$\gamma = N\lambda$

This is equal to the product of the tube length L (multiplied by two because the light passes through the tube twice) and the change in refractive index, Δn.

$\gamma = N\lambda = 2L(\Delta n)$

We can thereby solve:

$\Delta n = (N\lambda)/(2L)$

We know that the ratio between the starting and ending density define the starting and ending index of refraction. From the ideal gas law, we know density is proportional to pressure over temperature.

$\Delta\rho/\rho_0 = (\Delta n-1)/(n_0 -1) = (\Delta P T_0)/(P_0 \Delta T)$

Therefore, if we ensure $T=T_0$, we can solve:

$\Delta n = (n_0 -1)(\Delta P/P_0)$

Combining these equations, we can solve for n_0 our starting refractive index.

$\Delta n = (n_0 -1)(\Delta P/P_0) = (N\lambda)/(2L)$

$$\mathbf{n_0 = 1 + [(N\lambda)/(2L)]\,[P_0/\Delta P]}$$

Figure Three: An image of our Michelson Interferometer, overlaid with its schematic

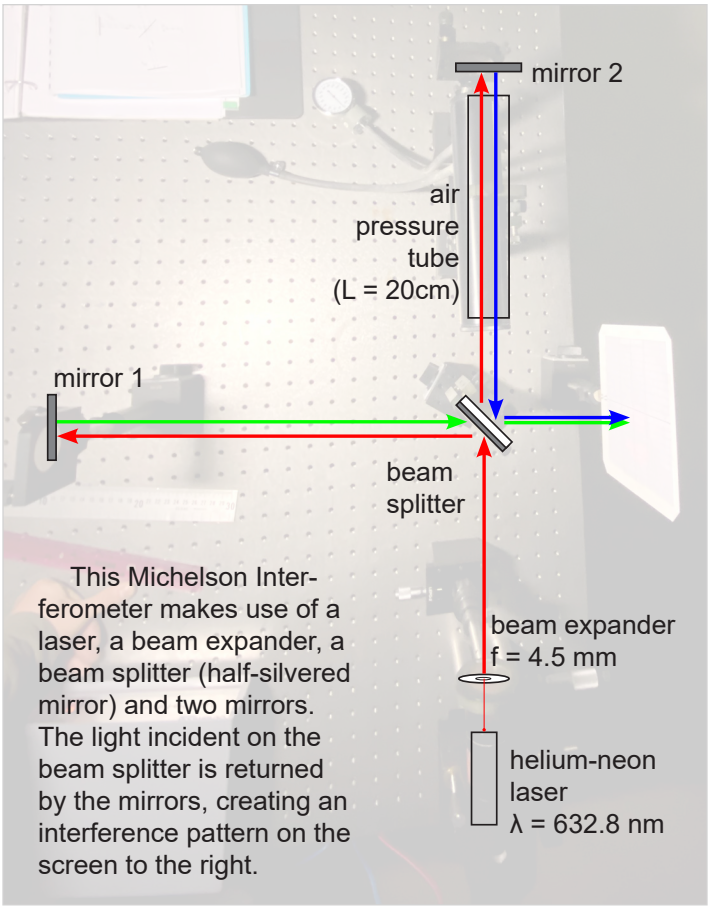

The Sagnac Interferometer

The Sagnac Interferometer has one major difference compared to the Michelson Interferometer, in that the light travels in a loop, rather than out and back.

In a stationary reference frame, the light from the beam splitter makes a simple lap around all the mirrors, arriving incident upon the beam splitter at its origin. If both arms are measured exactly, they meet each other in phase.

A factor of interest is that, if rotated, the path length of an individual light path will lengthen; the other will shorten (Sagnac, Georges). Take, for example, a clockwise spin. The light travelling clockwise (blue) will take less time to make the lap, due to the higher angular velocity. The light travelling counter-clockwise will experience the opposite.

Like the Michelson Interferometer, this interferometer was developed for the purpose of measuring Earth's movement relative to the Luminous Ether.

The Sagnac Interferometer is much more sensitive to the angles of the beam splitter and individual mirrors. It is imperative that each element be exactly 45 degrees to the beam, and that each 'side' of the loop be exactly the same length. Take care also to keep the beams parallel throughout their respective paths.

Since both beams of light travel through each segment, placing an air pressure tube anywhere does not vary the phase of each beam. Our table unfortunately does not rotate either, so we are unable to record any data for this interferometer. It is, however, schematically similar to the Mach-Zedner Interferometer and so, keeping all the elements on the table, we can make some easy modifications.

Figure Three: The Sagnac Interferometer, overlaid with its design schematic

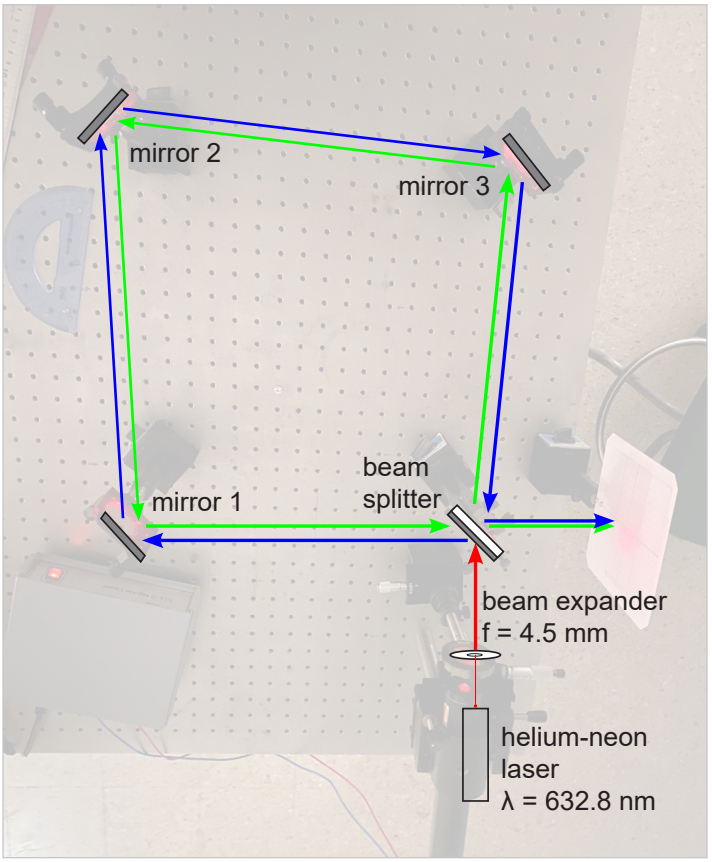

This Sagnac Interferometer makes use of a laser, a beam expander, a beam splitters (half-silvered mirror) and three mirrors. The light incident on the beam splitter is reflected across all three mirrors, returning to the original beam splitter to create an interference pattern.

This interferometer is designed to be rotated about the center to create an interference pattern, shortening and elongating the two light paths.

Figure Four: An interference pattern created by the Sagnac Interferometer

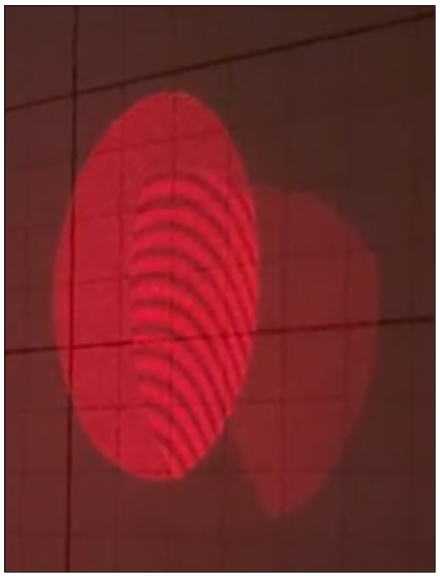

This beam, compared to the Michelson Interferometer pattern of Figure One, is much larger.

The light from the Sagnac Interferometer's beam splitter must travel roughly twice as long compared to the Michselson Interferometer before it returns to create an interference pattern.

The Mach-Zederman Interferometer

From a logistical perspective, the only difference between the Sagnac and Mach-Zedermen is a beam splitter and an extra screen. In fact, this is the easiest way to build this interferometer: starting first with the Sagnac to ensure that the beams are level and aligned, then substituting the second beam splitter for the last mirror. Figure Five shows this slightly different schematic.

Light that passes through the beam splitter reflects off a mirror on each arm and is coincident on a second beam splitter. This splitter then reflects and transmits two interference patterns. Each pattern is the inverse of the other -- fringes corresponding to troughs in the other, and vice versa.

A pressure tube can be placed in any segment between a mirror and beam splitter in order to collect data on the refractive index. The formula must be modified slightly, however, to account for the light travelling just once through the tube, we modify our Theorem One to be: $n_0 = 1 + [N\lambda/L] [P_0/\Delta P]$, removing a 1/2 factor on the second term.

The Mach-Zederman interferometer holds a couple benefits over the other interferometers on this list. For starters, its interference pattern is flat, as shown in Figure Six (a), compared to the circular patterns of the rest. This interferometer's wider and more stable beams also lend to the ability to visually demonstrate phase difference caused by items which are transparent but change the refractive index. When a flame is held up in front of a beam between either mirror and the last beam splitter, a pattern like Figure Six (b) appears. The clarity and clearly resolvable shape of these objects is unique to the Mach-Zederman interferometer.

Figure Five: The Mach-Zederman Interferometer, overlaid with its design schematic

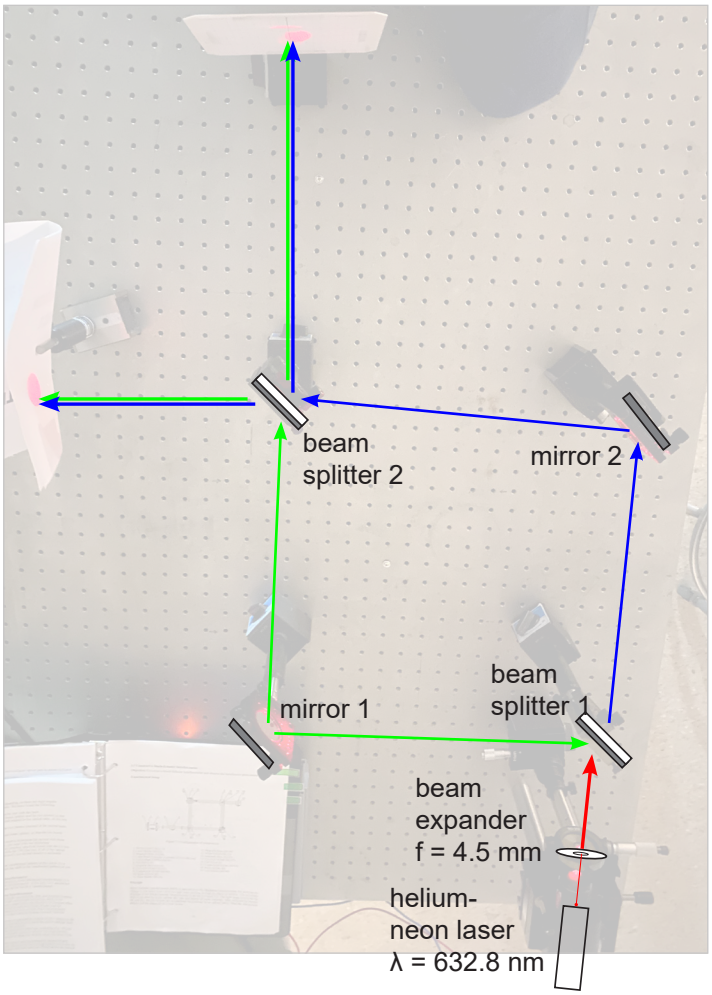

This Mach-Zederman Interferometer makes use of a laser, a beam expander, two beam splitters (half-silvered mirrors) and two mirrors.

Light from the first beam splitter is mirrored on both arms to the second beam splitter, creating an interference pattern.

Figure Six: Interference patterns created by the Mach-Zederman Interferometer

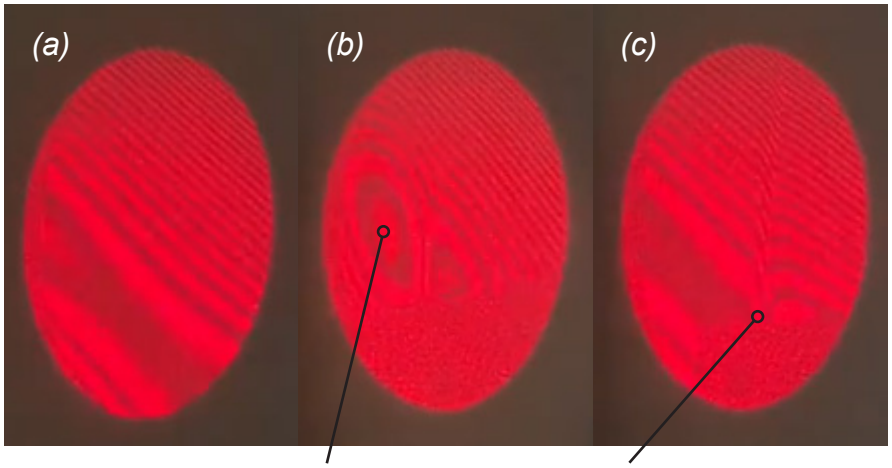

Without any changes, an interference pattern.

A lighter flame held in front of the beam.

A stream of butane held in front of the beam.

Three interference patterns created by the Mach-Zederman Interferometer. The Mach-Zederman is unique in that it can show clearly changes in refractive index of objects held before the beam.

The Fabry-Perot Interferometer

Our fourth interferometer differs greatly in form and function than the first three. We will use the Fabry-Perot Interferometer to measure the difference in wavelength of Sodium-D doublet interference lines.

Unlike the others, the Fabry-Perot interferometer uses incoherent light from a multimodal Sodium lamp. This light enters two half-silvered mirrors in parallel, allowing light to be 'trapped' in this cavity and reflects repeatedly until it escapes. This repeated reflection causes the light to interact and create an interference pattern.

Though, ideally, the lamp's rays are perpendicular to the first mirror, the incoherent nature of the light emitted by the lamp renders this relatively unnecessary. When calibrating the interferometer, it is actually more useful to set the mirrors parallel 'by eye.' Once they appear parallel, you can filter the lamp through a pinhole and attempt to line its tracers onto the same point. If this last step is done correctly, there should already be a shadow of interference over the pinhole. Removing the pinhole filter by this point will reveal the interference pattern, as shown in Figure Seven.

As the lamp is multimodal, we can sometimes observe a 'doublet' in the interference pattern, wherein there is a noticeable separation between the two wavelengths emitted by the lamp. This distance can be evaluated by changing the separation of the mirrors. As the mirror separation increases, the doublet will split, becoming blurry and converging until the lines begin to diverge and resolve clearly from one another again. This total mirror separation from divergence to convergence to divergence again is our recorded value for mirror separation $\Delta d = d_2 - d_1$.

To resolve the doublet, vary the mirror separation until the interference patterns begins to shift slightly. At this point, some tweaking of the mirrors may be required as the doublet begins to split and converge again. The image may become blurry throughout this process, especially if you are using a focusing lens. This is normal, as long as the image becomes clear as the doublet converges once again.

Figure Seven: The Fabry-Perot Interferometer

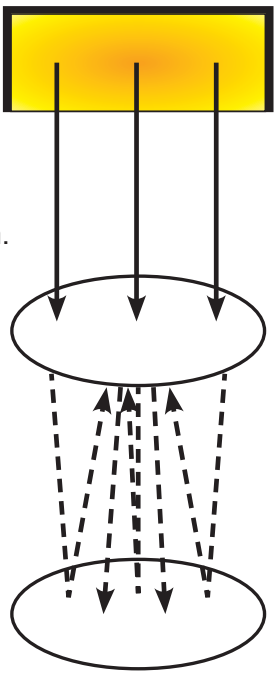

A sodium lamp emits incoherent light at two wavelengths: 589.0 and 589.5 nm.

Two half-mirrors in parallel allow light to be trapped in a 'Fabry-Perot cavity.'

Light that escapes creates an interference pattern.

The multimodal light of the Sodium lamp interferes with itself, creating a pattern. Varying the mirror separation t_q changes the relative phase difference $\Delta\lambda$ such that $t_q \propto 1/\Delta\lambda$.

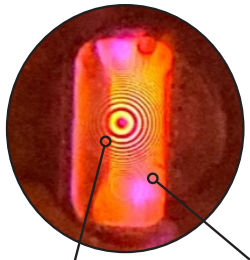

Doublet interference pattern

Sodium Lamp

With this principle in mind, we can develop a relationship to describe the difference between the doublet wavelengths ($\Delta\lambda$) by varying the mirror separation (Δd). Theorem Two does this, by involving the average of the doublet wavelengths (λ_k) to determine a theoretical value for the difference between the doublet wavelengths.

Error Analysis

Some discussion must specifically be had over the choice of error, its propagation, and our standards for determining whether our measurement is in good agreement with theory.

Firstly, with data we record ourselves, we determine its variance σ^2. With this, we are able to apply some error to the value. Say value x has a variance σ_x^2 -- its error will be $\sigma_x = \delta x$. We can represent this data set then as $x_i \pm \delta x_i$.

In all cases except one, this is how we will determine our error for collected data. This exception is the upper limit for our pressure value (ΔP). It was very difficult to accurately determine our starting pressure as the pressure tube we used had a leak. As such, high pressures were more difficult to accurately measure and time. For that reason, we assign our value $\Delta P = 300$ mmGHg ± 10 mmHg.

Many of our formulas are dependent on values assumed about the equipment we are using (e.g. the sodium lamp) and the environment (e.g. ambient air pressure). This includes the values we compare our When possible, we source these values from reputable or peer-reviewed sources. These sources are included in the bibliography.

Some information we collect does not include uncertainty due to the high precision of these experiments. In these, we include an uncertainty of $\pm 10^{-n}$ where n is the number of places the value includes. The refractive index of air, for example, we allow $n = 1.00027717 \pm 10^{-8}$.

When propagating error, we will use the rule of quadrature. For some function $q(x_1,x_2,...,x_i)$ with associated errors δx_i, the error for that function is $\delta(x_i) = \sqrt{(\sum(d/dx_i \times \delta x_i))}$.

We will then want to determine a weighted average to represent our data. First, the weight $w_i = 1/\sigma_i^2$. This is then used to compute the weighted average $x_{wAv} \pm \delta_{wAv} = (\sum w_i x_i)/(\sum w_i) \pm (\sum w_i)^{-1/2}$.

This value is important because we use its uncertainty to define our Gaussian Distribution. Composing this function is rather simple, requiring our computed and reference values and their included uncertainties.

Looking at Figure Eight, we see the equation for the Gaussian distribution, which defines its own error parameter σ and a center for the function, μ. We want to center our distribution at x = 0 so we choose μ = 0.

Theorem Two: Derivation of the relationship between Mirror and Doublet Separation

Diffuse light of wavelength λ that travels through the Fabry-Perot Interferometer with mirror separation Δd will leave at an angle θ_m such that:

$\cos(\theta_m) = [\lambda \times (m - \varphi/\pi)]/(2\Delta d)$

where φ is the phase of the light and m its order.

Light that has two wavelengths λ_1 and λ_2 produce between one and two rings per fringe, depending on the mirror separation.

At values of Δd where the rings coalesce into a single fringe, the innermost ring of λ_1 of order m overlaps the ring (m-1) of λ_2.

We equivalate these two states such that:

$[\lambda_1 \times (m - \varphi/\pi)]/(2\Delta d) = [\lambda_2 \times (m - 1 - \varphi/\pi)]/(2\Delta d)$

which solves to be:

$(\lambda_2 - \lambda_1)(m - \varphi/\pi) = \lambda_2 = \Delta\lambda(m - \varphi/\pi)$

Two assumptions are now made to simplify the equation further. First, because the Sodium-D lines are very closely spaced, we can say that the mean wavelength $\bar{\lambda} \approx \lambda_1 \approx \lambda_2$. Looking at the equation we have, the term $(m - \varphi/\pi)$ is dominated by m when it becomes large. Its largest value, achieved when the rings are closest to the axis of rotation -- essentially the center -- is $2\Delta d/\lambda$.

Replacing all the necessary components now, we get the following equation:

$\Delta\lambda(2\Delta d/\bar{\lambda}) = \bar{\lambda}$

which, solving for Δd:

$\Delta d = \bar{\lambda}^2/(2\Delta\lambda)$

Figure Eight: The Gaussian Distribution

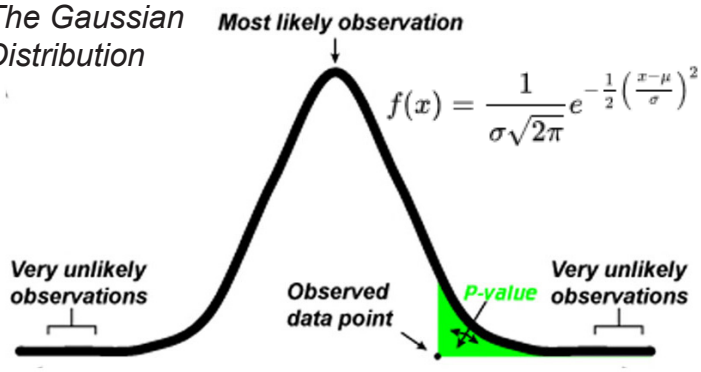

The Gaussian Distribution takes in our combined uncertainty to produce a distribution which evaluates the probabilistically 'best' value. With this, we can calculate the area under the curve from our data point (which will be the deviation from the accepted value) and find a p-value. This value helps us evaluate the accuracy of our experimental results.

(Stanford, 2016)

The parameter σ is simply defined as the propagation of the error in our weighted average and the reference value such that $\sigma = \sqrt{(\delta x_{wAv}^2 + \delta x_{ref}^2)}$.

The coefficient of the Gaussian Distribution normalizes the distribution, such that the integral over its full bounds (-∞,∞) is just one. For this reason, the p-value suggests a percent likelihood that a given value is correctly obtained.

Results

Calculating the Refractive Index of Air

We will be using three data sets to calculate the refractive index of air. From the Michelson Interferometer, we have two sets: one in which the arms are of equal length in Table One (a), and another with differing lengths in Table One (b). Our third set is from the Mach-Zederman Interferometer in Table One (c). All data tables are collated in the Appendix.

There are a few known values we need to consider before using Theorem One. First, the pressure. We started from an initial pressure P_0 =101.3 kPa and raised our tube pressure to about dP = 300 mmHg. As discussed in our error analysis section, our tube was leaking and so the exact pressure from which we started counting was difficult to ascertain. For this reason, we can consider our change in pressure dP = 300 ± 10 mmHg. This, of course, is converted to Pascals in our calculations.

Two slightly smaller considerations are the ratings provided to us for the tube length and the wavelength of the Helium-Neon laser. These we assign nominal uncertainties L = 20 ± 0.1 cm and λ = 632.8 ± 0.01 nm.

With these constants in mind, we run the data and recieve the sets shown in Figure Nine.

Taking this data, we can easily find the weighted averages of each of the sets:

Michelson Interferometer with equal-length arms: $(1 + 269.09 \times 10^{-6}) \pm (1.28 \times 10^{-6})$

Michelson Interferometer with differing-length arms: $(1 + 267.07 \times 10^{-6}) \pm (1.11 \times 10^{-6})$

Mach-Zederman Interferometer:
$(1 + 265.45 \times 10^{-6}) \pm (0.68 \times 10^{-6})$

Reference Value:
$(1 + 277.17 \times 10^{-6}) \pm (0.01 \times 10^{-6})$

Figure Nine: Comparing all calculated indexes against one another

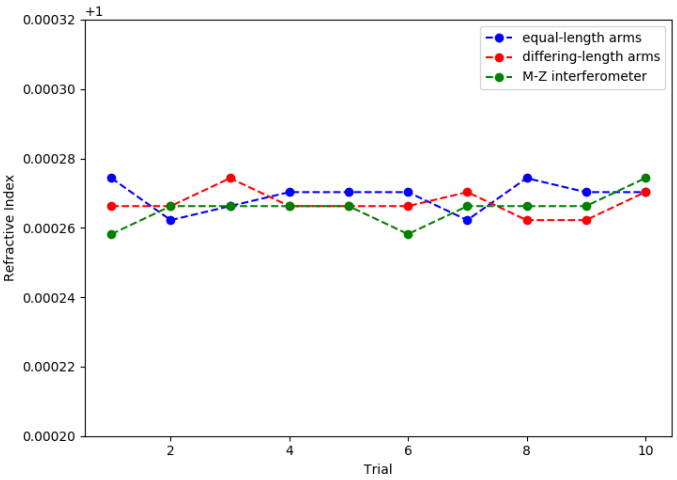

After applying our equation from Theorem One to all three data sets, we get this group of evaluations for the index of refraction. The blue and green dashed lines correspond to the equal- and differing-length Michelson Interferometer readings, respectively. The red corresponds to the Mach-Zederman Interferometer.

Figure Ten: The weighted averages of our data vs. our accepted value

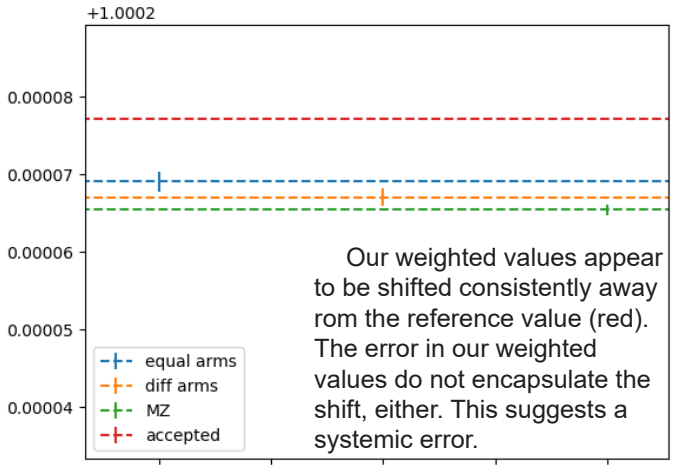

Placing our values side-by-side, there is a problem that is immediately evident. Our readings are shifted down, relative to the reference value we have for the index of refraction, as shown in Figure Ten. The error we have for each of these is very small, such that they do that include the reference value, though they do overlap slightly with each other.

The consistent shift downwards is indicative of a systemic issue, and with errors as small as those we have calculated, there isn't much wiggle room for the data.

Keeping in mind the considerable deviation from our expected value, the correspondent p-values for each of the values are practically zero. The orders for each of the p-values are 10^{-10}, 10^{-14} and 10^{-16} for the Michaelson interferometer with equal and differing arms and the Mach-Zederman interferometer, respectively.

The Spacing of Sodium-D Emission Lines

Unlike our single-mode laser from past interferometers, our light source is a multimodal Sodium lamp. The two wavelengths the lamp emits are 588.9950 and 589.5924 nanometers (Metrologia, Juncar). Given the already very high resolution of this measurement, we can consider the uncertainty for these values to be roughly the last digit: $\delta_\lambda = 0.0001 = 10^{-5}$.

For our purposes, we need their average as a 'known' wavelength $\lambda_k = 589.2937$ nm. We use this, and the equation from Theorem Two to evaluate the difference between the wavelengths in our analysis.

Computing all our data from Table Two, we get the following data shown in Figure Eleven. The data is largely consistent with only one outlier which does not skew the spread in a significant manner.

We can determine our theoretical value with which to compare using our known data: $(589.5924 - 588.9950) \pm (\delta_\lambda\sqrt{2})$ nm $= 0.5974 \pm (10^{-5}\sqrt{2})$ nm.

From here, we calculate a weighted average to represent our dataset. This weighted average turns out to be 0.5978 ± 0.0058 nm.

Taking these values -- the known and derived values and their respective uncertainties -- we can build our Gaussian Distribution. As shown in Figure Twelve, the weighted average value is in extremely good agreement with our expected measurements.

With our distribution, we can determine a p-value of 0.4698, meaning that we are very close to the probabilistically best measurement.

Figure Eleven: Calculated wavelength separation

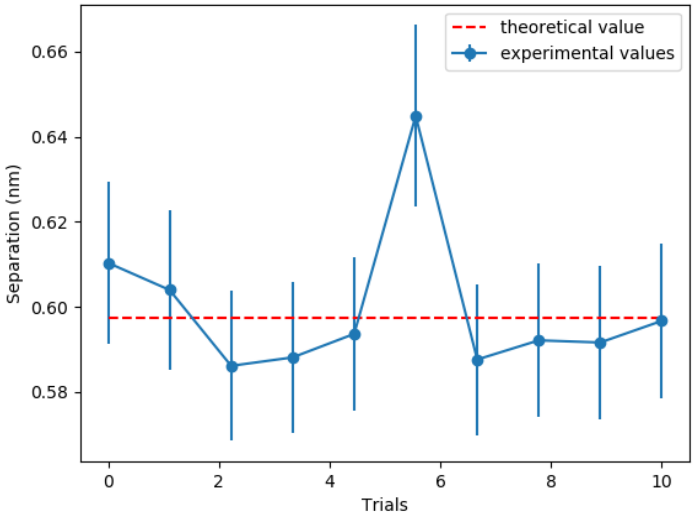

We run the data though Formula Two to find a calculated set for the wavelength separation (blue). Though there appears to be an outlier, the data we calculated tends to be rather close to the reference value (red) we have for the data.

Figure Twelve: Gaussian Distribution created around our weighted average value

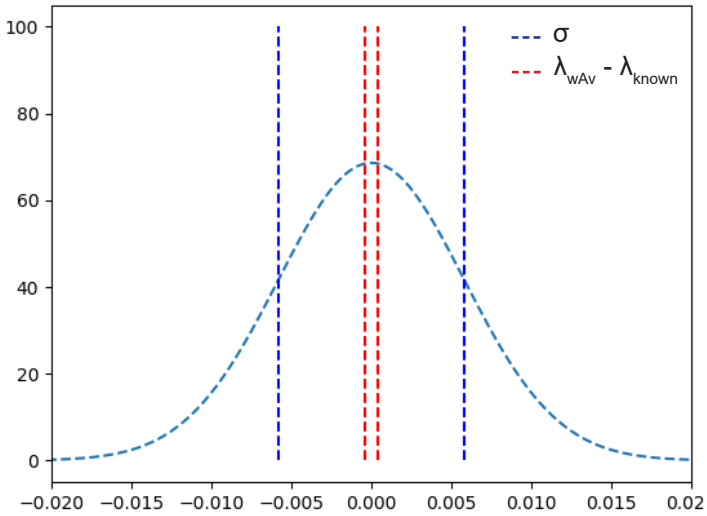

This Gaussian Distribution constructed around our weighted average value. The blue lines represent the first standard deviation from the mean whereas the red lines represent our value with respect to the mean.

Discussion

The goals of this report were to explore different variations of the interferometer, and to investigate the capabilities that each offered. From the Michelson to the Sagnac to the Mach-Zederman and, lastly, the Fabry-Perot interferometer, we were able to construct each with great precision and determine three independent values for the index of refraction and a remarkably accurate value for the separation of wavelengths of a Sodium-D light source.

Each of the interferometers' unique properties were researched and dicussed, and techniques specific to the construction of each were outlined -- hopefully to the benefit of future researchers.

Perhaps the most noticeable issue with the results of this report is the vast disagreement from the reference value for the index of refraction. The systemic shift suggests that there was a consistent error that affected this data. My hypothesis is the following:

When counting the fringes that passed for the interferometer, my lap partner pressurize the tube while I counted the fringes that passed. As it was difficult to exactly time when to start counting, I often chose to start counting as soon as the first interference pattern emerged and finish doing so with the last to emerge. The problem here is that, if I missed the end of one interference pattern and the beginning of another, that would constitute a full fringe. The systemic error could be the result of this small but albeit impactful method of recording data.

Regardless, more direct experimentation or a more rigorous analysis of our constants (e.g. recording air pressure) could yield more accurate results. The computed values were, after all, remarkably precise.

The weighted average for the spacing of sodium-D emission lines was shown to extremely accurate and precise. A p-value of 0.4698 constitutes a roughly 94% 'agreement.' For this reason, I would consider this part of the experiment successful.

Altogether, though the goals of the experiment were met. We were able to construct and calibrate a myriad of interferometers and describe their unique properties and specialized applications.

In the grander scheme of interferometry as a whole, it inspects a small portion of a field whose impact has been transformative on the whole of physics. Still yet, some appreciation and a deep understanding of the basics sheds light on the more complex versions of the same device. The same principles and features which govern these interfometers are what compose interferometers which have measured gravitational waves, scanned the galaxy and even surveyed the surface of another planet.

Appendix

Bibliography:

Feynman, Richard Philips. (1963-1965). The Feynman Lectures on Physics, Volume I. pg (15-3)-(15-5)

CalTech: LIGO's Interferometer. (Accessed January 29, 2020). Retrieved from https://www.ligo.caltech.edu/page/ligos-ifo

Brown, George. Physics 134 Advanced Laboratory Manual: Interferometery

Sagnac, Georges. Sur la preuve de la réalité de l'éther lumineux (1913). (Accessed January 29, 2020). Retrieved from https://fr.wikisource.org/wiki/Sur_la_preuve_de_la_réalité_de_l'éther_lumineux

Ciddor, Phillip E. Refractive index of air: new equations for the visible and near infrared (1996). Retrieved from https://www.osapublishing.org/ao/abstract.cfm?uri=ao-35-9-1566

P. Juncar, J. Pinard, J. Hamond, and A. Chartier, Metrologia 17, 77 (1981)

Source of Figure on page 8:
Dusheck, Jennie. Misleading p-values showing up more often in biomedical journal articles (2016). (Accessed January 29, 2020). Retrieved from http://med.stanford.edu/news/all-news/2016/03/misleading-p-values-showing-up-more-often-in-journals.html

Tables:

Table One

Trials	Number of Fringes Counted		
	Michelson, equal arms (a)	Michelson, different arms (b)	Mach-Zederman (c)
1	68	66	32
2	65	66	33
3	66	68	33
4	67	66	33
5	67	66	33
6	67	66	32
7	65	67	33
8	68	65	33
9	67	65	33
10	67	67	34

Table Two

Trials	d_1	d_2
1	12.850	18.540
2	12.650	18.400
3	12.835	18.760
4	12.625	18.530
5	12.870	18.720
6	13.100	18.485
7	12.640	18.550
8	12.945	18.810
9	12.720	18.590
10	12.670	18.490